Article

Structural and Thermodynamic Properties of Septin 3 Investigated by Small-Angle X-Ray Scattering

Maria Grazia Ortore,[1] Joci N. A. Macedo,[2] Ana Paula U. Araujo,[2] Claudio Ferrero,[3] Paolo Mariani,[1] Francesco Spinozzi,[1,*] and Rosangela Itri[4,*]

[1]Dipartimento di Scienze della Vita e dell'Ambiente and Consorzio Nazionale Interuniversitario per le Scienze Fisiche della Materia, Università Politecnica delle Marche, Ancona, Italy; [2]Instituto de Física de São Carlos, Universidade de São Paulo, São Carlos, Brazil; [3]European Synchrotron Radiation Facility, Grenoble, France; and [4]Instituto de Física da Universidade de São Paulo, São Paulo, Brazil

ABSTRACT Septins comprise a family of proteins involved in a variety of cellular processes and related to several human pathologies. They are constituted by three structural domains: the N- and C-terminal domains, highly variable in length and composition, and the central domain, involved in the guanine nucleotide (GTP) binding. Thirteen different human septins are known to form heterogeneous complexes or homofilaments, which are stabilized by specific interactions between the different interfaces present in the domains. In this work, we have investigated by in-solution small-angle x-ray scattering the structural and thermodynamic properties of a human septin 3 construct, SEPT3-GC, which contains both of both interfaces (G and NC) responsible for septin-septin interactions. In order to shed light on the role of these interactions, small-angle x-ray scattering measurements were performed in a wide range of temperatures, from 2 up to 56°C, both with and without a nonhydrolysable form of GTP ($GTP_{\gamma}S$). The acquired data show a temperature-dependent coexistence of monomers, dimers, and higher-order aggregates that were analyzed using a global fitting approach, taking into account the crystallographic structure of the recently reported SEPT3 dimer, PDB:3SOP. As a result, the enthalpy, entropy, and heat capacity variations that control the dimer-monomer dissociation equilibrium in solution were derived and $GTP\gamma S$ was detected to increase the enthalpic stability of the dimeric species. Moreover, a temperature increase was observed to induce dissociation of SEPT3-GC dimers into monomers just preceding their reassembling into amyloid aggregates, as revealed by the Thioflavin-T fluorescence assays.

INTRODUCTION

Septins belong to a family of guanine nucleotide binding proteins, which were first identified in *Saccharomyces cerevisiae* as essential for the completion of the cell cycle (1). Septins are filament-forming proteins and considered as a novel component of cytoskeleton (2). Although they are absent in higher plants, septins are highly conserved in eukaryotes, where the number of septin genes ranges from 1 in *Chlamydomonas reinhardtii* to 13 in humans (3). In addition to the role in cytokinesis, several functional studies have shown the involvement of septins in a variety of key cellular processes, including synaptic vesicle trafficking (4), microtubule regulation (5), exocytosis (6), membrane dynamics, and DNA repair (7). Besides their physiological functions, recent reports have related the septins to several neuropathologies (8–10), cancers (11–13), and infectious diseases (14,15). However, the specific molecular role of septins in these human disorders remains unclear.

Septins comprise three conserved structural domains as schematized in Fig. 1. The N- and C-terminal domains are highly variable in length and amino acid (aa) composition. Most of the septins present a sequence at the C-terminal, which is predicted to form a coiled-coil and has been suggested to mediate septin-septin interactions, thus controlling filament formation (16,17).The central core of septins is formed by a guanine-nucleotide (GTP) binding domain that shares at least three conserved motifs exhibiting the P-loop of GTPases (18,19). Usually, a polybasic region, which has been shown to bind membrane phospholipids (20,21), is present at the interface between the N-terminal and the GTP binding domains. The binding to GTP and its hydrolysis were experimentally demonstrated for several septins (22,23), and crystallographic and biochemical studies have suggested nucleotide binding to play a role in the regulation of SEPT2 filament assembly (24).

Based on sequence similarity, the 13 human septins are classified into four subgroups: SEPT2, SEPT3, SEPT6, and SEPT7. Various studies demonstrated that septins of distinct subgroups can associate to form complexes with variable composition, and these complexes assemble into filaments and higher-order structures (24–26). The complex formed by septins 2, 6, and 7 is the only one whose three-dimensional x-ray structure is available. The order of the subunits in this structure is 7-6-2-2-6-7 and was obtained in sufficient detail to show that the complex assembly was dependent on the GTPase domains. GDP is present in septins and capable of homotypic interaction, and GTP is the nucleotide bound to the partners in the heterotypic interactions (26).

Submitted December 23, 2014, and accepted for publication May 11, 2015.

*Correspondence: f.spinozzi@univpm.it or itri@if.usp.br

Editor: James Cole.

0006-3495/15/06/2896/7 $2.00

http://dx.doi.org/10.1016/j.bpj.2015.05.015

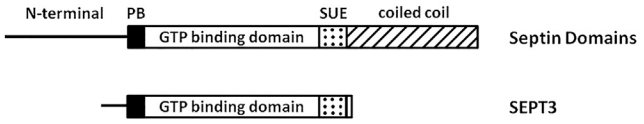

FIGURE 1 Schematic representation of the typical septin structure. Septin domains include a highly conserved GTP-binding domain, which is flanked by a variable N-terminal and a C-terminal amino-acid sequence usually predicted as a coiled-coil domain. A polybasic sequence (*PB*) interacts with phospholipids. The septin unique element (*SUE*) is also represented. Since major variations in septins are in the length and amino-acid composition of their N- and C-terminal domains, we represent SEPT3 for comparison, too.

Recent studies have proposed that SEPT9 (which belongs to the SEPT3 group) can occupy the end position in the 7-6-2-2-6-7 hexamer configuration forming an octamer, like the one observed in yeast septins (27,28). In addition to the heterofilaments, a few septin homofilaments have been observed in vivo (22,29,30). Some homofilaments in vitro have been characterized as being amyloidlike fibers (31,32).

This study focuses on SEPT3, which is a brain-tissue-specific protein. Its phosphorylation by cGMP-dependent protein kinase can regulate its subcellular localization (33). Similarly to some other septins, SEPT3 is associated with several pathologies, such as Alzheimer disease, Down syndrome, mesial temporal lobe epilepsy, and brain tumors (2,9,13). To date, mammalian SEPT3 is described to form a complex with SEPT5 and SEPT7. However, this composition has been questioned and a misannotation to the copurified septins was advanced (34,35). SEPT3 presents some interesting particularities: it belongs to the only group of human septins that possess no coiled-coil in the C-terminal domain (Fig. 1) and was obtained as a nucleotide-free monomer.

Recently, some of us investigated a construct of human SEPT3, which was purified as a nucleotide-free monomer and included the GTP-binding as well as the C-terminal domain. This construct was termed SEPT3-GC (23). In the crystal structure, SEPT3-GC forms foreshortened filaments (23), which employ the same NC and the nucleotide binding site interfaces (G interfaces) observed in the hetero-complex of human septins 7-6-2-2-6-7. Notably, this characteristic has been related to SEPT2 and SEPT7, supporting the concept of promiscuous interactions, in which a septin could self-assemble into homofilaments (i.e., lacks a binding partner) (23,36). In solution, its monomeric state was stated to be closely correlated with the absence of a Tyr residue in the position 282, which in the SEPT3 group is replaced by a Thr residue. Solely the single mutation T282Y was enough to lead to the dimerization of SEPT3 (23).

As many different combinations of the 13 human septins are theoretically possible, it is important to comprehend the structural basis of a specific filament assembly. In the case of SEPT3-GC in solution, the results from size-exclusion chromatography revealed that the construct elutes predominantly as a monomer in the absence of nucleotide bound, at salt concentrations varying from 50 to 300 mM NaCl at 20°C (23). For $GTP_{\gamma}S$ in Mg^{2+}-containing saline buffer solution, the elution profiles of SEPT3-GC are consistent with monomers and dimers coexisting in solution, providing strong evidence that the G interface is responsible for the dimer formation. Furthermore, the dimer-monomer equilibrium is displaced for higher salt concentrations (23).

In this work, we combine small-angle x-ray scattering (SAXS) and Thioflavin (ThT) experiments to follow the changes of SEPT3-GC monomer-dimer equilibrium in solution toward the formation of amyloid fibrils upon temperature increase, in the absence and presence of $GTP_{\gamma}S$. By applying a unique fitting procedure to the SAXS data of the same sample recorded at different temperatures, we are able to derive thermodynamic parameters directly from the scattering curves and, hence, to evaluate the enthalpic and entropic contributions in the septin assembly/disassembly.

MATERIALS AND METHODS

Materials

SEPT3-GC expression and purification were performed as reported in Macedo et al. (23). Experiments were performed on SEPT3-GC defined by residues 59–350, thus lacking the SEPT3 N-terminal but linked with a 23-aa-long His-TAG, comprising a molecular mass of 36 kDa. Previous attempts to express and purify the full-length SEPT3 resulted in complex samples containing various oligomeric states (23). The protein construct was dissolved in a solution of 40 mM Tris, 300 mM NaCl, 5 mM $MgCl_2$, and 1 mM 2-mercaptoethanol, 10% glycerol, pH 7.8 at a concentration of 5.4 gL^{-1}. $GTP_{\gamma}S$ was purchased from Sigma-Aldrich (St. Louis, MO) and used without purification. 450 μM $GTP_{\gamma}S$ was added to the SEPT3-GC solution. The mutant T282Y was also obtained following the preparation reported in Macedo et al. (23).

SAXS

SAXS experiments were performed at the BioSAXS beamline of the European Synchrotron (ESRF) in Grenoble, France. The sample-to-detector distance was set to 1.803 m and the available q range ($q = 4\pi\sin\Theta/\lambda$, where 2Θ is the scattering angle and λ is the x-ray wavelength) spanned between 0.01 and 0.42 $Å^{-1}$. Each sample exposure time was 160 s, which ensured enough statistical accuracy without degrading the samples by radiation. Samples were handled using a robotic sample changer equipped with a temperature control. A Pilatus 1-M detector was used (37). The SAXS curves were normalized by taking into account the transmitted x-ray beam intensity. The scatterings of the buffer and empty cell were subtracted according to standard procedures. A solution of bovine serum albumin of known concentration was employed to produce data on an absolute scale, i.e., the macroscopic differential scattering cross section, $I(q)$.

SAXS spectra from SEPT3-GC in solution, both in the presence and in the absence of $GTP_{\gamma}S$, were measured at temperatures between $T = 2$°C and 56°C.

Previous size-exclusion chromatography results suggested the presence of monomers and dimers in equilibrium solution at room temperature (23). Accordingly, $I(q)$ can be written as

$$I(q) = \frac{cN_A}{M_1}\left[x_1P_1(q) + \frac{1}{2}(1-x_1)P_2(q)\right], \qquad (1)$$

where c is the protein weight concentration, N_A is the Avogadro number, M_1 is the SEPT3-GC monomer molecular weight, and x_1 is the fraction of monomers in solution. $P_1(q)$ and $P_2(q)$ are the monomer (hereafter named SEPT3-GC_1) and the dimer (SEPT3-GC_2) form factors, respectively. They are calculated on the basis of the available crystallographic structure of the dimer (see below) by taking into account the flexibility of N- and C-terminal ends; the protein thermal expansivity $\alpha_T = \partial \log V/\partial T$ (as described in Ortore et al. (38)); the contribution of the solvation shell, the mass density of which is supposed to be different from the one of the bulk solvent (actually, the parameter considered in the calculation is the mass density of the solvation shell relative to the mass density of the bulk water). Finally, the solvent scattering length density was calculated as a function of composition and temperature, according to the standard molecular volume of each component.

Concerning the monomer SEPT3-GC_1 and dimer SEPT3-GC_2 structures, both were based on the recently resolved dimer crystal structure of the human SEPT3-GC construct (PDB:3SOP, 60–329 aa in the monomer) (23). However, a number of residues were not located in the crystallographic results, while the SEPT3-GC of our SAXS experiment included a 23-aa-long His-TAG at the N-terminal and a 21-aa chain at the C-terminal. A specific software, described in detail in the Supporting Material, was thus developed to generate two batches of 100 atomic structures. These batches correspond to monomers SEPT3-GC_1 and dimers SEPT3-GC_2, taking into account the SEPT3 primary structure (His-TAG + 59-350 aa), having as a template the PDB:3SOP and allowing random conformations of all the residues not located in the crystallographic structure. For each conformer, the SAXS form factor was calculated using the SASMOL approach (38) included in the GENFIT code (39), which finds the water molecules in contact with protein species and assigns to them a relative mass density different from the one of water molecules in the bulk. Three sets of representative atomic structures of monomers and dimers are shown in Fig. 2, together with the form factors $P_1(q)$ and $P_2(q)$ of all the monomer and dimer conformations of the two batches. Of note, the set of functions does not significantly deviate from the average value, represented by the curves shown in black. These curves indicate that the behavior of the form factor is mainly due to the rigid core of the protein and is only slightly modified by the flexibility of the terminal chains, which involve 21% of all the amino acids. As a consequence, the analysis of experimental SAXS curves has been carried out with monomer and dimer form factors averaged over the two batches of conformations (*black curves* in Fig. 2).

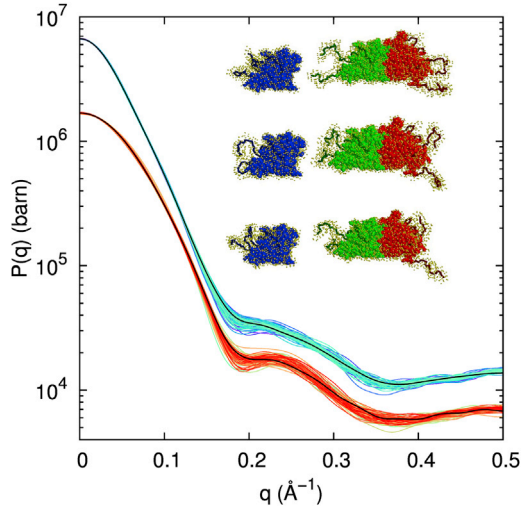

FIGURE 2 Form factors of SEPT3-GC_1 monomers (*red curves*) and SEPT3-GC_2 dimers (*cyan curves*) corresponding to 100 conformations of each species obtained by using the 3SOP crystallographic structure as template, including the construct primary amino-acids sequence (59–350 aa), the HisTag linked with the N-terminal domain and other missing residues. Three representative conformations (*blue*, *green*, and *red*) of monomers and dimers are shown. (*Darker colors*) The HisTag, the 21-aa chain at the C-terminal, and the other missing residues. (*Yellow spheres*) Hydration water molecules in contact with the protein surface. Form factors are calculated with SASMOL (38), with the relative mass density of hydration water set to 1.05.

ThT fluorescence assay

Aliquots of 8 μM nucleotide-free SEPT3GC, bound to 25 μM GTPγS, were incubated with 50 μM ThT. Excitation was performed at 450 nm on a K2 spectrofluorimeter (ISS, Champaign, IL) using a 1 cm pathlength quartz cuvette. ThT emission was monitored at 482 nm for 5400 s. Measurements were performed at 25, 38, 47, 50, and 56°C. Data points were analyzed with the software ORIGINPRO 8.0 (OriginLab, Northampton, MA).

RESULTS AND DISCUSSION

Fig. 3 presents SAXS curves from SEPT3-GC in 300 mM NaCl buffer solution, measured both in the presence and the absence of GTP$_\gamma$S at $T = 2$°C and $T = 20$°C, respectively. It can be noted that the SAXS curves obtained without GTP$_\gamma$S differ from those with GTP$_\gamma$S: in particular, the curves are comparable for $q > 0.1$ Å^{-1}, but significantly different for $q < 0.1$ Å^{-1}, where the presence of GTP$_\gamma$S induces an increase in the intensity. The values of $I(0)$ obtained by extrapolating the data through the Guinier's law (40) at low q angles amount to 0.049 ± 0.002 and 0.074 ± 0.001 cm^{-1}, respectively, for septin in the absence and presence of the nucleotide. Because the scattering at zero angle, $I(0)$, is proportional to the mean molecular weight of the scattering object (41), the results indicate that GTP$_\gamma$S promotes increase in the average size of SEPT3-GC species in solution. In fact, the presence of monomers and dimers in equilibrium in solution, for both temperatures, will be shown in the further sections.

In order to extract information on the structural properties, the SAXS curves measured up to 56°C are displayed as a Kratky plot ($q^2I(q)$ versus q; see Fig. 4). Such a diagram is very useful, because the whole protein conformation can be easily characterized: in particular, the visual inspection of the Kratky representation helps differentiate between compact and unfolded conformations or to highlight the presence of intermediate partially unfolded states (38,41). For SEPT3-GC in solution, the bell-shaped profile observed up to 38°C (Fig. 4) indicates a folded protein conformation. In complement, Fig. 5 displays the results of ThT assays performed on SEPT3-GC up to 5400 s. As one can see, at 25°C no significant emission of ThT was verified in the absence or in the presence of GTPγS. At 38°C, there is a slow increase in the ThT fluorescence versus time, more evident in the absence of the nucleotide, suggesting the formation under this condition of amyloidlike aggregates with time. Of

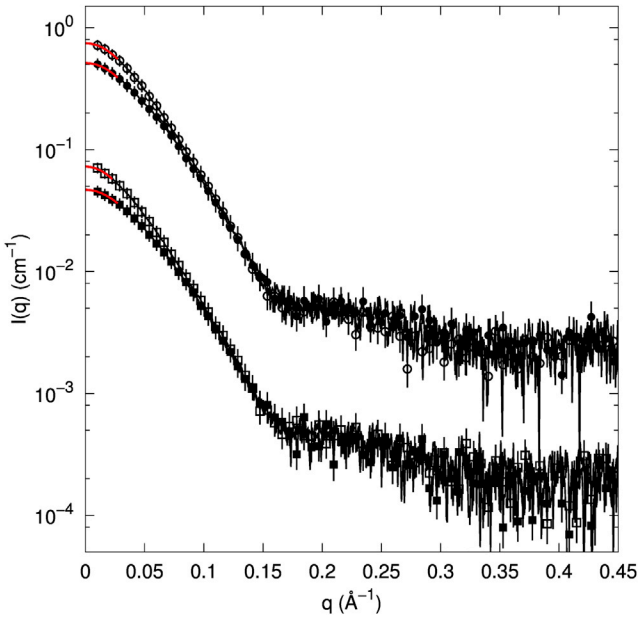

FIGURE 3 SAXS curves from SEPT3-GC in the absence (*solid symbols*) and presence of GTPγS (*open symbols*) at 2°C (*squares*) and 20°C (*circles*). Curves pertaining to samples at 20°C are shifted up by a factor 10 for the sake of clarity. (*Solid lines*) Best fittings to the SAXS curves according to Guinier's law at low q values (see text for details). To see this figure in color, go online.

note, SAXS data were taken in the first minutes of the experiments and, hence, agree with no-formation of amyloidlike aggregates at 38°C for short time intervals.

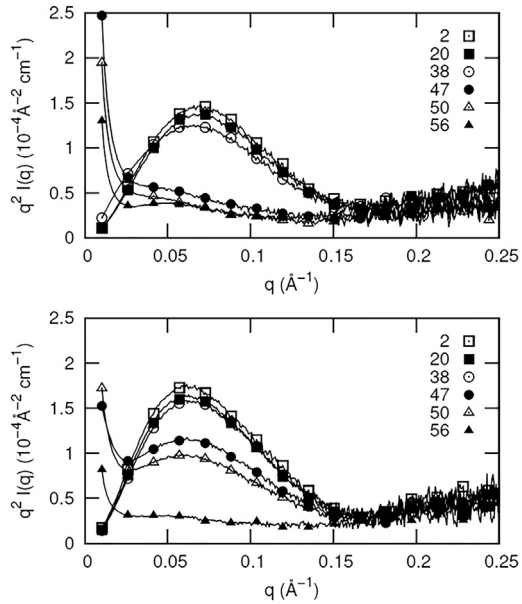

FIGURE 4 Kratky plots of SEPT3-GC in solution. (*Top*) SEPT3-GC in the standard buffer without GTPγS; (*bottom*) buffer with 450 μM GTPγS. (*Right-hand-side number in each frame*) Temperatures investigated in °C. For the sake of clarity, only few symbols of the data points are shown.

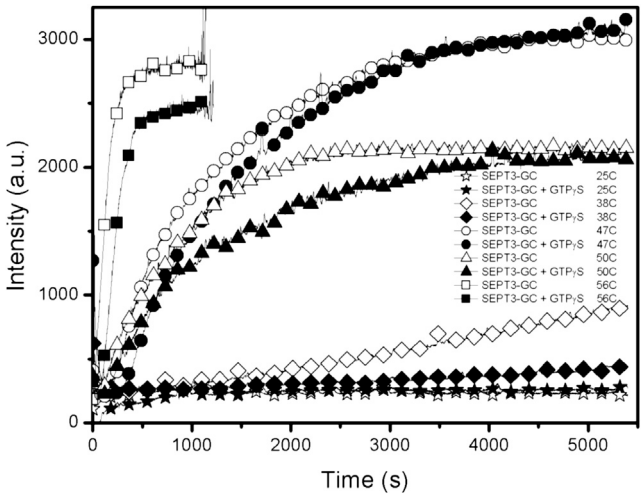

FIGURE 5 ThT fluorescence assay. Fluorescence emission intensity values from ThT in the presence of 8 μM nucleotide-free SEPT3GC (*open symbols*), bound to 25 μM GTPγS (*solid symbols*) at different temperatures reported in the legend, were monitored at 482 nm, after excitation at 450 nm. At 56°C, the proteins precipitated after ~1000 s.

Interestingly, there is a marked transition between 38 and 47°C, characterized by the depression of the bell-shaped profile along with a significant increase of the scattering intensity in the small q range in the SAXS Kratky representation (Fig. 4), accordingly with ThT results (Fig. 5). There is a rapid increase of ThT fluorescence intensity in the first minutes of SEPT3-GC incubation at 47 and 50°C (Fig. 5), a clear indication of amyloidlike fibrils formation. It should be noted, however, that this process is faster in the absence of the nucleotide than in its presence. Moreover, such a difference is more prominent at 50°C. Such findings are parallel to the marked depression of the bell-shape profile in the Kratky representation (Fig. 4, *top*) from septin in nucleotide-free solution. Therefore, at the temperature range between 38 and 47°C, SEPT3-GC evolves quickly to amyloidlike aggregates that must be long enough to produce high scattering intensities at low q values (see comparison with numerical simulations reported in Fig. S2 in the Supporting Material). On the other hand, in the presence of GTPγS, Kratky plots (Fig. 4, *bottom*) point out that some amount of smaller nonamyloid aggregates up to 50°C (in accordance with results reported on Fig. S2) coexists in solution with amyloidlike aggregates, due to a continuous reduction of the bell-like peak above 40°C.

In order to better investigate the features of the nonamyloid septin aggregates present in solution at low temperatures, we now resort to the analysis of the SAXS curves. In a previous article, a SAXS curve from SEPT3-GC at 20°C, dispersed in a similar buffer solution but containing a large amount of salt (800 mM NaCl), showed that the protein was in a monomeric state in the solution (23). The behavior of the SAXS data collected in this investigation at 300 mM NaCl is not compatible with the presence of

only monomeric septins, even at low T. In this way, the low T SAXS curves were thus analyzed by attributing the scattered intensity to the contribution of monomers and dimers (Fig. 2) in equilibrium solution, according to Eq. 1.

The fraction of monomers x_1 in solution is related to the thermodynamics of the temperature-induced dissociation process of SEPT3-GC. In fact, this process can be described in terms of the dissociation equilibrium constant, $K_{\rm dis}$, and the corresponding dissociation free energy, $\Delta G_{\rm dis}$, such that

$$K_{\rm dis} = \frac{[SEPT3GC_1]^2}{[SEPT3GC_2]} = e^{-\Delta G_{\rm dis}/k_{\rm B}T} = \frac{2cx_1^2}{(1-x_1)M_1}, \quad (2)$$

where $k_{\rm B}$ is the Boltzmann constant. Rearranging Eq. 2, x_1 can be written as

$$x_1 = \frac{M_1 e^{-\Delta G_{\rm dis}/k_{\rm B}T}}{4c}\left[\left(1+\frac{8c}{M_1}e^{\Delta G_{\rm dis}/k_{\rm B}T}\right)^{1/2}-1\right]. \quad (3)$$

The T-dependence of the free energy can be expressed in terms of variations of dissociation enthalpy ($\Delta H^0_{\rm dis}$) and entropy ($\Delta S^0_{\rm dis}$) at the reference temperature $T_0 = 298$ K as well as of the variation of the heat capacity ($\Delta C_{P,\rm dis}$):

$$\Delta G_{\rm dis} = \Delta H^0_{\rm dis} - T\Delta S^0_{\rm dis} + \Delta C_{P_{\rm dis}}\left(T - T_0 - T\log\frac{T}{T_0}\right). \quad (4)$$

Equation 4 can be used to derive a relation between x_1 and $\Delta H^0_{\rm dis}$, $\Delta S^0_{\rm dis}$, and $\Delta C_{P\rm dis}$. As a result, each set of the scattering curves obtained at temperatures preceding the formation of amyloid aggregates (e.g., 32°C in the absence of GTPγS and 44°C in the presence of GTPγS, for a total of 8 and 10 curves, respectively) has been analyzed using a unique fitting procedure aimed to derive the unknown structural factors (namely, the relative mass density d of the solvation shell and the thermal expansivity factor α_T) and the thermodynamic parameters ($\Delta H^0_{\rm dis}$, $\Delta S^0_{\rm dis}$, and $\Delta C_{p\rm dis}$). The analysis was performed using GENFIT (39). Fig. 6 shows the best theoretical fits to the experimental data, whereas Fig. 7 displays the monomer fractions x_1, calculated both in the absence and presence of GTPγS via Eq. 3. The fitting parameters are summarized in Table 1.

The quality of the fitting curves (Fig.4) is very good, considering the values of the global reduced χ^2 ranging from 0.9 and 1.0 (according to the χ^2 definition reported in Spinozzi et al. (39)). We also measured the SEPT3GC mutant (T282Y), which is known to be a dimer in solution (23). The corresponding experimental data along with the fitting curve is the uppermost one reported on the right-hand panel of Fig. 6. The fitting strategy in this case was similar to the generally adopted one, confirming the presence of only dimeric species for these mutants in solution.

Regarding the temperature dependence of the SEPT3-GC monomeric state in solution, Fig. 7 reveals that ~50% of

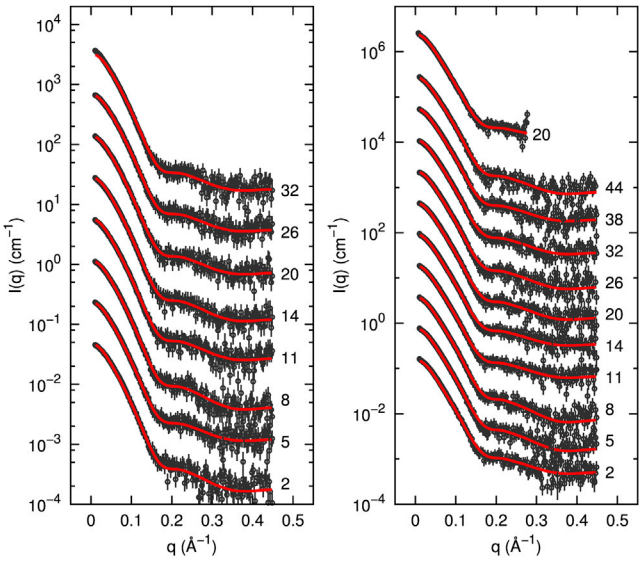

FIGURE 6 Experimental SAXS curves and theoretical best-fit results (*continuous red lines*). SAXS spectra from samples with 5.4 g L^{-1} SEPT3-GC concentration. (*Left*) Solution without GTPγS. (*Right*) Solution with 450 μM GTPγS. The uppermost curve refers to the SEPT3-GC mutant T282Y (see text for details). The numbers on the right-hand side of each picture denote the investigated temperatures in °C. The curves are scaled by a factor 5 for the sake of clarity. To see this figure in color, go online.

monomers coexist with dimers up to 20°C in 300-mM NaCl-containing buffer solution without GTPγS, whereas a small fraction of dimers dissociate into monomers with temperature increase up to $T = 32$°C. Conversely, in the presence of GTPγS, most of SEPT3GC is a dimer up to 20°C, and a small amount of dissociation occurs as the temperature increases. The results thus indicate in both cases that a fraction of the dimers dissociates into monomers preceding amyloid fibrils formation identified by ThT fluorescence

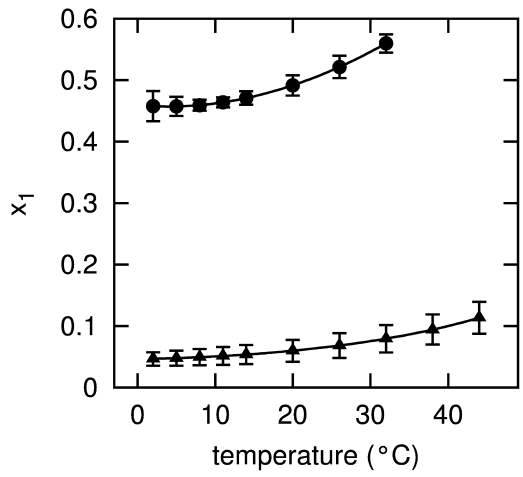

FIGURE 7 Monomer fraction versus temperature. (*Circles*) Data collected from the sample without GTPγS; (*triangles*) data collected from the sample with the addition of 450 μM GTPγS.

TABLE 1 Fitting parameters

	ΔH^0_{dis} (kJ mol^{-1} K^{-1})	ΔS^0_{dis} (kJ mol^{-1} K^{-1})	ΔC_{Pdis} (kJ mol^{-1} K^{-1})	ΔG_{dis}[a] (kJ mol^{-1} K^{-1})	d	α_T (10^{-4} K^{-1})
Native	23.9 ± 0.4	1.0 ± 0.8	1.1 ± 0.6	23.6 ± 0.4[b]	1.10 ± 0.01	1.4 ± 0.1
450 μM GTPγS	35 ± 2	1.0 ± 0.8	1.1 ± 0.6	35 ± 2[b]		
Mutant T282Y				38 ± 7		

[a]Values at $T = 20°C$.
[b]Values calculated from Eq. 4.

data (Fig. 7). Previous results from septin 4 (31) and septin 2 (32) showed that they have a tendency to aggregate rapidly by forming amyloid structures dependent on the temperature. Additionally, analysis in silico of all human septins (32) defined one amyloidogenic region in a GTP-binding domain, which is characteristic of the human septins.

Based on that, one could suggest that the dissociation of SEPT3-GC as a function of temperature could be related to a rearrangement of the secondary structure allowing for the amyloid fibrils assembling, which was evidenced by ThT experiments. Protein dissociation preceding a reassembling into an amyloidlike configuration has also been recently reported on glyceraldehyde-3-phosphate dehydrogenase, which is a homotetramer in its native state (42).

As to the fitting parameters, Table 1 shows that a unique value of the relative mass density of the solvation shell is sufficient to fit all the low-T curves in any conditions of GTPγS. Likewise, a unique value for the thermal expansivity is also adequate to fitting the whole data. Moreover, the value found for α_T is in agreement with the one of met-myoglobin (43), and significantly smaller than the one commonly stated for folded proteins (44).

The dissociation free energy was found to be different in the two experimental conditions, but readily comparable to the solvation free energy loss, $\Delta G = 41$ kJ mol^{-1}, as calculated by the PISA program from the PDB coordinates of SEPT3-GC (23). The dependence on GTPγS is very interesting: in fact, while the solvation shell properties and protein thermal expansivity should depend uniquely on SEPT3-GC features, one would expect that the GTPγS presence should affect the thermodynamic parameters, ruling the monomer-dimer equilibrium. However, both the dissociation entropy and the difference of heat capacity resulted to be independent of the presence of GTPγS (see Table 1). The difference between the two conditions is indeed found only in the dissociation enthalpy: in the absence of GTPγS, $\Delta H_{dis}{}^0$ is 23.9 ± 0.4 kJ mol^{-1} K^{-1}, whereas it amounts to 35 ± 2 kJ mol^{-1} K^{-1} when GPTγS is present. This finding clearly indicates that GTPγS raises the enthalpic stability of the dimeric species.

Therefore, our SAXS data coupled with a careful thermodynamic analysis strongly support the conclusion that the GTPγS binding favors SEPT3-GC dimerization at low temperatures. Furthermore, the data also suggest that when heating septin, amyloid structures formation may be preceded by dimer dissociation into monomers. Such findings could play an important role in secondary structure changes that might result in formation of septin amyloidlike fibrils above the physiological temperature.

SUPPORTING MATERIAL

Supporting Materials and Methods and two figures are available at http://www.biophysj.org/biophysj/supplemental/S0006-3495(15)00500-7.

AUTHOR CONTRIBUTIONS

M.G.O. acquired and analyzed the data; J.N.A.M. prepared the sample and performed ThT assays; A.P.U.A. designed research and wrote the article; C.F. acquired the data; P.M. designed research; F.S. acquired the data, wrote the software to analyze the data, and wrote the article; and R.I. designed research, analyzed the data, and wrote the article.

ACKNOWLEDGMENTS

We are grateful of Adam Round at the European Synchrotron Radiation Facility for providing assistance in using the BioSAXS beamline.

A.P.U.A. and R.I. are recipients of The National Council for Scientific and Technological Development (Brazil) research fellowships. J.N.A.M. received a scholarship from the São Paulo Research Foundation.

REFERENCES

1. Hartwell, L. H. 1971. Genetic control of the cell division cycle in yeast. IV. Genes controlling bud emergence and cytokinesis. *Exp. Cell Res.* 69:265–276.
2. Mostowy, S., and P. Cossart. 2012. Septins: the fourth component of the cytoskeleton. *Nat. Rev. Mol. Cell Biol.* 13:183–194.
3. Nishihama, R., M. Onishi, and J. R. Pringle. 2011. New insights into the phylogenetic distribution and evolutionary origins of the septins. *Biol. Chem.* 392:681–687.
4. Tsang, C. W., M. Fedchyshyn, …, W. S. Trimble. 2008. Superfluous role of mammalian septins 3 and 5 in neuronal development and synaptic transmission. *Mol. Cell. Biol.* 28:7012–7029.
5. Nagata, K., A. Kawajiri, …, M. Inagaki. 2003. Filament formation of MSF-A, a mammalian septin, in human mammary epithelial cells depends on interactions with microtubules. *J. Biol. Chem.* 278:18538–18543.
6. Beites, C. L., H. Xie, …, W. S. Trimble. 1999. The septin CDCrel-1 binds syntaxin and inhibits exocytosis. *Nat. Neurosci.* 2:434–439.
7. Kremer, B. E., L. A. Adang, and I. G. Macara. 2007. Septins regulate actin organization and cell-cycle arrest through nuclear accumulation of NCK mediated by SOCS7. *Cell.* 130:837–850.
8. Kinoshita, A., M. Kinoshita, …, J. Kimura. 1998. Identification of septins in neurofibrillary tangles in Alzheimer's disease. *Am. J. Pathol.* 153:1551–1560.

9. Takehashi, M., T. Alioto, …, K. Ueda. 2004. Septin 3 gene polymorphism in Alzheimer's disease. *Gene Expr.* 11:263–270.
10. Ihara, M., H. Tomimoto, …, M. Kinoshita. 2003. Association of the cytoskeletal GTP-binding protein Sept4/H5 with cytoplasmic inclusions found in Parkinson's disease and other synucleinopathies. *J. Biol. Chem.* 278:24095–24102.
11. Capurso, G., T. Crnogorac-Jurcevic, …, G. Delle Fave. 2005. Peanut-like 1 (septin 5) gene expression in normal and neoplastic human endocrine pancreas. *Neuroendocrinology.* 81:311–321.
12. Montagna, C., M. S. Lyu, …, T. Ried. 2003. The Septin 9 (MSF) gene is amplified and overexpressed in mouse mammary gland adenocarcinomas and human breast cancer cell lines. *Cancer Res.* 63:2179–2187.
13. Kim, D. S., S. L. Hubbard, …, J. T. Rutka. 2004. Analysis of mammalian septin expression in human malignant brain tumors. *Neoplasia.* 6:168–178.
14. Cossart, P., J. Pizarro-Cerdá, and M. Lecuit. 2003. Invasion of mammalian cells by *Listeria monocytogenes*: functional mimicry to subvert cellular functions. *Trends Cell Biol.* 13:23–31.
15. Tran Van Nhieu, G., E. Caron, …, P. J. Sansonetti. 1999. IpaC induces actin polymerization and filopodia formation during Shigella entry into epithelial cells. *EMBO J.* 18:3249–3262.
16. Casamayor, A., and M. Snyder. 2003. Molecular dissection of a yeast septin: distinct domains are required for septin interaction, localization, and function. *Mol. Cell. Biol.* 23:2762–2777.
17. de Almeida Marques, I., N. F. Valadares, …, R. C. Garratt. 2012. Septin C-terminal domain interactions: implications for filament stability and assembly. *Cell Biochem. Biophys.* 62:317–328.
18. Bourne, H. R., D. A. Sanders, and F. McCormick. 1991. The GTPase superfamily: conserved structure and molecular mechanism. *Nature.* 349:117–127.
19. Field, C. M., and D. Kellogg. 1999. Septins: cytoskeletal polymers or signaling GTPases? *Trends Cell Biol.* 9:387–394.
20. Zhang, J., C. Kong, …, W. S. Trimble. 1999. Phosphatidylinositol polyphosphate binding to the mammalian septin H5 is modulated by GTP. *Curr. Biol.* 9:1458–1467.
21. Damalio, J. C., T. M. Nobre, …, A. P. Araújo. 2013. Lipid interaction triggering Septin2 to assembly into β-sheet structures investigated by Langmuir monolayers and PM-IRRAS. *Biochim. Biophys. Acta.* 1828:1441–1448.
22. Huang, Y. W., M. C. Surka, …, W. S. Trimble. 2006. GTP binding and hydrolysis kinetics of human septin 2. *FEBS J.* 273:3248–3260.
23. Macedo, J. N., N. F. Valadares, …, A. P. Araújo. 2013. The structure and properties of septin 3: a possible missing link in septin filament formation. *Biochem. J.* 450:95–105.
24. Sirajuddin, M., M. Farkasovsky, …, A. Wittinghofer. 2009. GTP-induced conformational changes in septins and implications for function. *Proc. Natl. Acad. Sci. USA.* 106:16592–16597.
25. Nagata, K., T. Asano, …, M. Inagaki. 2004. Biochemical and cell biological analyses of a mammalian septin complex, Sept7/9b/11. *J. Biol. Chem.* 279:55895–55904.
26. Sirajuddin, M., M. Farkasovsky, …, A. Wittinghofer. 2007. Structural insight into filament formation by mammalian septins. *Nature.* 449:311–315.
27. Nakahira, M., J. N. Macedo, …, J. Kobarg. 2010. A draft of the human septin interactome. *PLoS ONE.* 5:e13799.
28. Kim, M. S., C. D. Froese, …, W. S. Trimble. 2011. SEPT9 occupies the terminal positions in septin octamers and mediates polymerization-dependent functions in abscission. *J. Cell Biol.* 195:815–826.
29. Mendoza, M., A. A. Hyman, and M. Glotzer. 2002. GTP binding induces filament assembly of a recombinant septin. *Curr. Biol.* 12:1858–1863.
30. Kim, M. S., C. D. Froese, …, W. S. Trimble. 2012. Uncovering principles that control septin-septin interactions. *J. Biol. Chem.* 287:30406–30413.
31. Garcia, W., A. P. de Araújo, …, R. C. Garratt. 2007. An intermediate structure in the thermal unfolding of the GTPase domain of human septin 4 (SEPT4/Bradeion-β) forms amyloid-like filaments in vitro. *Biochemistry.* 46:11101–11109.
32. Pissuti Damalio, J. C., W. Garcia, …, A. P. Ulian Araújo. 2012. Self assembly of human septin 2 into amyloid filaments. *Biochimie.* 94:628–636.
33. Xue, J., C. W. Tsang, …, P. J. Robinson. 2004. Septin 3 (G-septin) is a developmentally regulated phosphoprotein enriched in presynaptic nerve terminals. *J. Neurochem.* 91:579–590.
34. Lukoyanova, N., S. A. Baldwin, and J. Trinick. 2008. 3D reconstruction of mammalian septin filaments. *J. Mol. Biol.* 376:1–7.
35. Sellin, M. E., L. Sandblad, …, M. Gullberg. 2011. Deciphering the rules governing assembly order of mammalian septin complexes. *Mol. Biol. Cell.* 22:3152–3164.
36. Sellin, M. E., S. Stenmark, and M. Gullberg. 2014. Cell type-specific expression of SEPT3-homology subgroup members controls the subunit number of heteromeric septin complexes. *Mol. Biol. Cell.* 25:1594–1607.
37. Pernot, P., A. Round, …, S. McSweeney. 2013. Upgraded ESRF BM29 beamline for SAXS on macromolecules in solution. *J. Synch. Radiat.* 20:660–664.
38. Ortore, M. G., F. Spinozzi, …, D. Russo. 2009. Combining structure and dynamics: non-denaturing high-pressure effect on lysozyme in solution. *J. Roy. Soc. Interface.* 6 (*Suppl 5*):S619–S634.
39. Spinozzi, F., C. Ferrero, …, P. Mariani. 2014. GENFIT: software for the analysis of small-angle x-ray and neutron scattering data of macro-molecules in solution. *J. Appl. Cryst.* 47:1132–1139.
40. Guinier, A., and G. Fournet. 1955. Small Angle Scattering of X-Rays. Wiley, New York.
41. Barbosa, L. R., F. Spinozzi, …, R. Itri. 2013. Proteins in Solution and at Interfaces. J. M. Ruso and A. Pineiro, editors John Wiley, New York, pp. 49–72.
42. Ávila, C. L., C. M. Torres-Bugeau, …, R. N. Chehin. 2014. Structural characterization of heparin-induced glyceraldehyde-3-phosphate dehydrogenase protofibrils preventing α-synuclein oligomeric species toxicity. *J. Biol. Chem.* 289:13838–13850.
43. Frauenfelder, H., H. Hartmann, …, N. Max. 1987. Thermal expansion of a protein. *Biochemistry.* 26:254–261.
44. Dellarole, M., K. Kobayashi, …, C. A. Royer. 2013. Probing the physical determinants of thermal expansion of folded proteins. *J. Phys. Chem. B.* 117:12742–12749.